Generalized scintillation detection and ranging results obtained by use of a modified inversion technique

Rachel A. Johnston, Christopher Dainty, Nicholas J. Wooder, and Richard G. Lane

The measurement of the strength of atmospheric optical turbulence by use of a modified generalized SCIDAR (scintillation detection and ranging) inversion technique is outlined and demonstrated. This new method for normalizing and inverting scintillation covariances incorporates the geometry specific to generalized SCIDAR. Examples of profiles from two astronomical observation sites are presented.

OCIS codes: 100.3190, 280.7060.

1. Introduction

Atmospheric turbulence severely degrades the quality and resolution of images captured by ground-based telescopes. Although adaptive optics techniques can compensate for the distortion introduced by the atmosphere in real time, compensation is achieved only over a small angular region around the reference object known as the isoplanatic patch. The isoplanatic patch describes the angle of the sky over which the distortion that is due to turbulence can be considered to be unchanging, thus limiting the extent of objects that can be imaged. By use of multiconjugate adaptive optics it is possible to perform a three-dimensional correction of the turbulence to increase the field of view over which compensation can be achieved. These techniques are greatly assisted by knowledge of the vertical turbulence structure.[1,2]

SCIDAR (scintillation detection and ranging), proposed by Vernin and Roddier in 1973,[3] is a remote-sensing technique that is used to estimate the refractive-index structure constant as a function of altitude $C_n^2(h)$, which gives a direct measure of the vertical turbulence profile. The geometry of this problem is illustrated in Fig. 1. The normalized scintillation variance, σ_I^2, is proportional to the 5/6th power of altitude, so for short propagation distances σ_I^2 is barely detectable. In the original method the scintillation is measured at the telescope aperture, hence it is blind to low-altitude turbulence and so does not provide a complete turbulence profile.

By shifting the measurement plane optically beneath the telescope, the low-altitude turbulence now gains an additional propagation distance in which to increase to a measurable strength. This technique, proposed by Fuchs *et al*. in 1994[4] and implemented by Avila *et al*. in 1997,[5] is referred to as generalized SCIDAR and can be extended to include an estimate of the velocity profile as well.[6,7] The geometry of this problem, illustrated in Fig. 2, is more complicated than the SCIDAR geometry, since the observed image now consists of two defocused and overlapped pupil images.

The SCIDAR and generalized SCIDAR techniques involve the capture of a large number of binary star scintillation patterns, calculation of the average normalized scintillation autocovariance in real time[5,8] or by postprocessing[6] captured and recorded scintillation patterns, and extraction of the atmospheric optical turbulence profile by solving an integral inversion. In a matrix formulation, the atmospheric optical turbulence profile $C_n^2(h)$ is related to the scintillation autocovariance as

$$S(\rho) = T(\rho, h)C_n^2(h) + n(\rho), \tag{1}$$

where ρ is the physical distance in the measurement plane. Here $T(\rho, h)$ represents the kernel, which is made up of theoretical autocovariance[9] for a range of altitudes. $S(\rho)$ is a one-dimensional slice of the two-dimensional normalized average scintillation covariance calculated from the observed scintillation

R. A. Johnston (Johnston_ra@hotmail.com) and C. Dainty are with the Blackett Laboratory, Imperial College, London SW7 2BX, UK. N. J. Wooder is with the Technology Partnership, Melbourn Science Park, Royston, SG8 6EJ, UK. R. G. Lane is with the Department of Electrical and Electronic Engineering, University of Canterbury, Private Bag 4800, Christchurch, New Zealand.

Received 22 November 2001; revised manuscript received 6 June 2002.

0003-6935/02/326768-05$15.00/0

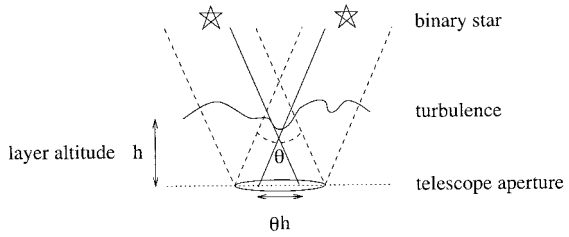

Fig. 1. SCIDAR geometry.

frames and $n(\rho)$ is the measurement noise. The aim is to invert the measured scintillation covariance to obtain an estimate of the turbulence profile $C_n^2(h)$.

Many of the parameters used to characterize atmospheric turbulence can then be calculated from the estimated $C_n^2(h)$.[6] For example, the Fried parameter or turbulence coherence length r_0 is related to $C_n^2(h)$ as

$$r_0 = \left[0.42k^2 \sec(z) \int C_n^2(h) \mathrm{d}h \right]^{-3/5}, \qquad (2)$$

where k is the wave number and z is the zenith angle. Since r_0 can also be measured by other means, this provides a way to verify the calculated C_n^2 values.

Typically the normalization for both SCIDAR and generalized SCIDAR data have been performed identically. However, in this manner, the estimation of turbulence profiles and the corresponding r_0 values by use of Eq. (2) produced values for the turbulence strength that were inconsistent with the atmospheric conditions observed at the time the data were captured. Hence the motivation for this research has been the desire to obtain C_n^2 and r_0 values that are consistent with the seeing at their time of capture.

The existing and new generalized SCIDAR normalization methods are explained in Section 2. Section 3 contains a brief description of the setup used to obtain experimental SCIDAR data at the astronomical observation sites considered. Application of the new normalization to experimental SCIDAR data is presented in Section 4. Finally, conclusions are presented in Section 5.

2. Theory

The SCIDAR technique is based on calculation of the average normalized autocovariance of a large number of short-exposure scintillation images produced by a binary star. In addition, dark count and background measurements should be incorporated at this stage of the calculation. The theoretical autocovariance of crossed-beam (binary star) scintillation data, in the case of generalized SCIDAR, is a function of both spatial and angular variables and is denoted by $C_B(\rho, \theta)$, where

$$C_B(\rho, \theta) = \sum_h \left(\frac{1 + \alpha^2}{(1 + \alpha)^2} C_S(\rho) + \frac{\alpha}{(1 + \alpha)^2} \times \{ C_S[\rho - \theta(h + d)] + C_S[\rho + \theta(h + d)] \} \right). \qquad (3)$$

Here $C_S(\rho)$ is the theoretical scintillation autocovariance that is due to a single star, α is the relative magnitude of the binary star, and $\theta(h + d)$ is the separation of scintillation patterns that is due to each individual star, where h represents the distance from the turbulent layer to the telescope aperture and d is the distance of defocus beneath the telescope. $C_S(\rho)$ is obtained by Hankel transformation of the spatial power spectrum of the scintillation $W_S(f)$, where[9]

$$W_S(f) = 0.039k^2 f^{-11/3} \int_0^\infty C_N^2(h) \sin(\pi \lambda h f^2) \mathrm{d}h. \qquad (4)$$

The separation of the pupil images that is due to each component of the binary star is given by θd (see Fig. 2). The observed image for a single turbulent layer at ground level ($h = 0$) is given by

$$y(\rho) = [m(\rho) + s(\rho)] + \alpha[m(\rho + \theta d) + s(\rho + \theta d)]. \qquad (5)$$

Although the image described by Eq. (5) depends on a two-dimensional vector $\boldsymbol{\rho}$, only the modulus of the vector is considered, without loss of generality. The first terms, $[m(\rho) + s(\rho)]$, correspond to the image that is due to the first binary star pupil components, where $m(\rho)$ represents the mean pupil data and $s(\rho)$ represents the zero mean scintillation pupil data. The remaining terms represent the image formed from the second binary star pupil components, displaced from the first images by an amount proportional to the defocus distance. Note that, for $h = 0$, Eq. (5) is an equality. For ($h > 0$) this expression becomes an approximation since the atmosphere that the light from each star passes through is slightly different. The average ensemble autocovariance is

$$\begin{aligned} C_B'(\rho) &= \langle y(\rho) * y(\rho) \rangle - \langle y(\rho) \rangle * \langle y(\rho) \rangle \\ &= \langle y(\rho) * y(\rho) \rangle - \langle [m(\rho) + \alpha m(\rho + \theta d)] \\ &\quad * [m(\rho) + \alpha m(\rho + \theta d)] \rangle \\ &= (1 + \alpha^2) \langle s(\rho) * s(\rho) \rangle + \alpha [\langle s(\rho) \\ &\quad * s(\rho + \theta d) \rangle + \langle s(\rho) * s(\rho - \theta d) \rangle], \end{aligned} \qquad (6)$$

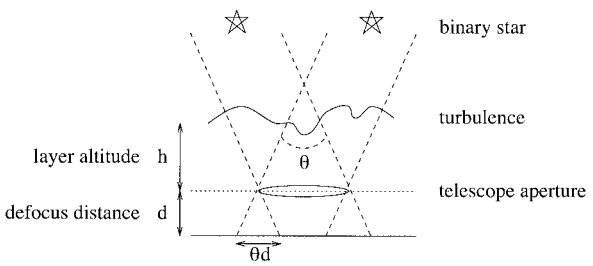

Fig. 2. Generalized SCIDAR geometry.

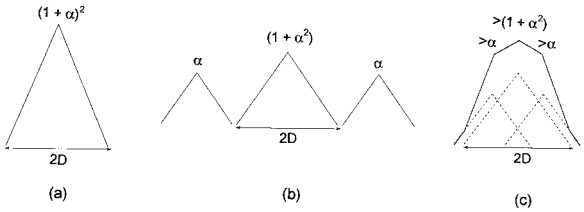

Fig. 3. Normalization functions for (a) $\theta d = 0$, (b) $\theta d > 2D$, (c) $\theta d < 2D$.

where the $*$ denotes the correlation operation. The existing method for normalizing the autocovariance is to divide by the autocorrelation of the mean signal:

$$(1 + \alpha^2)\langle m(\rho) * m(\rho)\rangle + \alpha[\langle m(\rho) * m(\rho + \theta d)\rangle + \langle m(\rho) * m(\rho - \theta d)\rangle]. \quad (7)$$

For conventional SCIDAR the defocus distance d is zero. Thus $\theta d = 0$ so the terms in expression (7) are identical, i.e., $\langle m(\rho) * m(\rho)\rangle = \langle m(\rho) * m(\rho + \theta d)\rangle = \langle m(\rho) * m(\rho - \theta d)\rangle$. As a result they completely overlap as shown in Fig. 3(a). In this case the normalization is performed correctly as Eq. (6) over expression (7) is equal to $C_B(\rho, \theta)$ [see Eq. (3)]. If θd is greater than twice the width of scintillation pattern D, the terms in expression (7) do not overlap; see Fig. 3(b). Hence the normalization performed is equivalent to dividing each term in Eq. (6) by the corresponding normalization term given in expression (7). When $\theta d < 2D$, the terms in expression (7) partially overlap, as in Fig. 3(c). In this case the normalization is performed incorrectly, different regions of the normalized covariance are too small whereas others remain unchanged. This underestimation of the covariance results in r_0 estimates that are too large. Nearly all the experimental generalized SCIDAR data corresponds to $0 < \theta d < 2D$, hence the straightforward inversion used in the original SCIDAR method is inappropriate.

The correct normalization of the generalized SCIDAR covariances requires that each of the individual normalization terms is extracted. Theoretically one can achieve this by performing a deconvolution of the function described by expression (7) with

$$\frac{(1 + \alpha^2)}{\alpha}\,\delta(\rho) + \delta(\rho - \theta d) + \delta(\rho + \theta d) \quad (8)$$

to obtain an estimate of $\langle m(\rho) * m(\rho)\rangle$. An alternative to deconvolution is to image a single star simultaneously to obtain $\langle m(\rho) * m(\rho)\rangle$. In either case, the estimated $\langle m(\rho) * m(\rho)\rangle$ can then be scaled and shifted as required for the normalization of each term in Eq. (6).

Although the correct normalization of the autocovariance data by dividing by the extracted normalization term produces an unbiased autocovariance result, the division significantly amplifies any noise that is present. This is more of a problem at larger shifts that correspond to higher altitudes as there is a smaller area of overlap of the pupil images that is due to each component of the binary star, hence the average is over a much smaller area. The traditional approach is to solve Eq. (1). However, a better approach is to solve[10]

$$S'(\rho) = T'(\rho, h)C_n^2(h) + n(\rho), \quad (9)$$

where $T'(\rho, h)$ is defined by

$$T'(\rho, h) = T(\rho, h)\langle m(\rho) * m(\rho)\rangle, \quad (10)$$

thus avoiding the need for division of S' in the normalization of the experimental scintillation autocovariances. T' is intuitively more reasonable as less weighting is given to higher altitudes that are averaged over a much smaller area and that correspond to a smaller degree of pupil overlap.

Assuming Gaussian noise, a maximum-likelihood approach to the inversion of Eq. (1) reduces it to the well-known least-squares formulation. Tyler and Steinhoff[11] show that the profile of the atmosphere can be obtained from SCIDAR measurement data by minimization of the least-squares error function

$$E = \|T'(\rho, h)C_n^2(h) - S'(\rho)\|^2. \quad (11)$$

However, the problem is inherently ill-conditioned and as a result its inversion can lead to unacceptable noise amplification. A practical solution requires prior information in the form of regularization, where regularization is a statement of the energy or smoothness of the solution. The positivity of the turbulence profile $C_n^2(h)$ provides an additional constraint. This positively constrained deconvolution problem was reformulated as a quadratic programming problem and was solved by use of an accelerated quadratic programming technique that incorporated Tikhonov–Miller regularization.[12]

Simulations were performed to determine the accuracy of this method. Two simulation examples are discussed here. In each case a single turbulent layer at ground level ($h = 0$) was simulated. The first example was a binary star of 5-arc sec separation propagated over a defocus distance of 2 km, and the second example was a 10-arc sec separation binary star defocused over a distance of 5 km. In each example a telescope diameter of 0.5 m was assumed. The simulated turbulence strength for each example was 2.1×10^{-13} m$^{-2/3}$, corresponding to an r_0 of 25 cm. Inversion of the average scintillation autocovariances from an ensemble of 1000 scintillation frames produced a single layer at ground level for each sample problem with r_0 values of 24.7 and 22.6 cm, respectively.

3. Experimental Setup

The optical system used to acquire experimental SCIDAR data is illustrated in Fig. 4. The imaging system consists of an image intensifier fiber coupled to a high speed 128×128 pixel DALSA CCD camera. The digital output from the DALSA camera is acquired by a Bitflow Raptor PCI frame capture board controlled by a fast PC, and the data are stored directly onto digital linear tape.

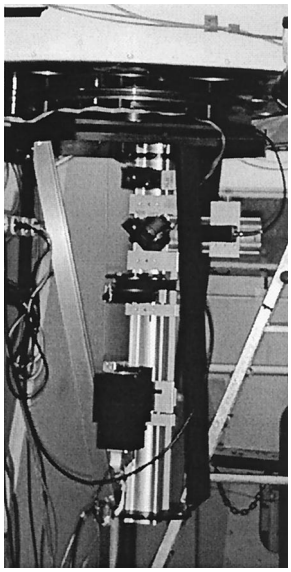

Fig. 4. Experimental Setup.

A field lens was used to ensure that the pixel sampling in the pupil plane image was approximately 1 cm $\times$ 1 cm. For operation in a generalized SCIDAR mode, this field lens was replaced by a lens of a different focal length to move the measurement plane optically beneath the telescope (see Fig. 5).

4. Results

The new inversion method was applied to real scintillation data from two astronomical observation sites. The observation sites considered are Mount John, New Zealand (McLellan 1 m), in April 1999 and Calar Alto, Spain (1.23 m), in June–July 2001.

Figure 6 illustrates unnormalized autocovariance slices for each observation site. Each part of the figure shows two or three (consecutive) autocovariances, each calculated from 2000 scintillation frames, where the first autocovariance is shown as a solid curve, the second as a dashed curve, and where there is a third as a dotted curve. The $C_n^2(h)$ profiles estimated from these autocovariances are illustrated in Fig. 7. The two sets of profiles appear similar to previously published $C_n^2(h)$ profiles[6] in form. Each

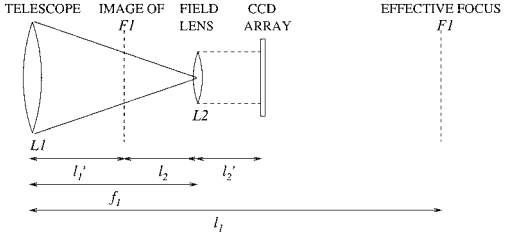

Fig. 5. Schematic diagram of the SCIDAR optical system. When the system is operated in the conventional SCIDAR mode, field lens $L2$ is selected to produce an image of the desired size at the CCD, fixing l_2' for operation in both generalized and conventional SCIDAR modes. Operation in the generalized SCIDAR mode simply requires a change of field lens. The location of the virtual measurement plane is then given by use of the thin-lens equation.

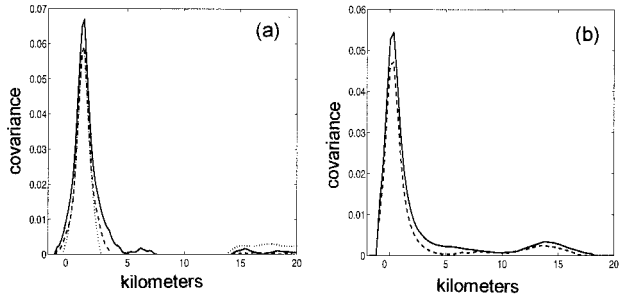

Fig. 6. Scintillation covariances from (a) Mount John and (b) Calar Alto.

profile is dominated by boundary-layer turbulence, with definite high-altitude turbulence appearing between 10 and 15 km in each case.

The fit to the experimental data is very good, as illustrated in Fig. 8. We confirmed the reliability of these results by numerically calculating the root-mean-square (rms) error of the solution, using a method similar to that in the paper by Kluckers *et al.*[6] Let $\epsilon\{S - \hat{S}\}$ represent the rms error between the true data S and the covariance function obtained from the estimated profile $\hat{C}_n^2(h)$, i.e., $\hat{S} = T\hat{C}_n^2(h)$. Here $\epsilon\{S - \hat{S}\}$ is defined as

$$\epsilon\{S - \hat{S}\} = \sqrt{\frac{\langle (S - \hat{S})^2 \rangle}{\langle S^2 \rangle}}. \tag{12}$$

The rms of the solution, $\epsilon\{C_n^2(h) - \hat{C}_n^2(h)\}$, cannot be calculated directly. It can, however, be approxi-

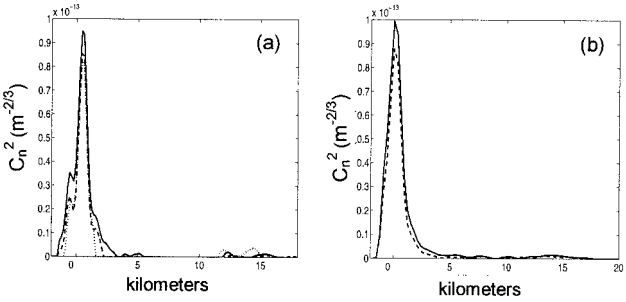

Fig. 7. Consecutive $C_n^2(h)$ profiles from (a) Mount John and (b) Calar Alto.

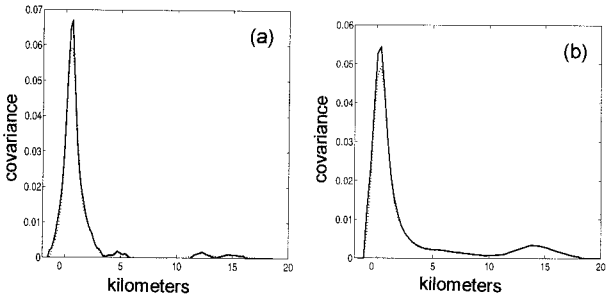

Fig. 8. Fit (dotted curve) to data (solid curve) for sample profiles from (a) Mount John and (b) Calar Alto.

Table 1. r_0 Estimates in Centimeters

Profile	Mount John	Calar Alto
1	10.7	12.6
2	12.8	14.8
3	13.3	—

mated by $\epsilon\{\hat{C}_n^2(h) - C_n^2(h)^P\}$, where $C_n^2(h)^P$ is a randomly perturbed version of $\hat{C}_n^2(h)$, i.e.,

$$C_n^2(h)^P = \hat{C}_n^2(h) + \beta W. \quad (13)$$

Here W represents random Gaussian noise and β is the noise weighting. The weighting of the random perturbation is increased until $\epsilon\{\hat{S} - S_P\} = \epsilon\{S - \hat{S}\}$. When this occurs $\epsilon\{\hat{C}_n^2(h) - C_n^2(h)^P\}$ represents a reasonable approximation to $\epsilon\{C_n^2(h) - \hat{C}_n^2(h)\}$. The rms error of each $C_n^2(h)$ profile shown is estimated to be within 5% for the Calar Alto profiles and within 10% for the Mount John profiles.

The r_0 values associated with each of the profiles are summarized in Table 1. It is obvious that the strengths of the profiles illustrated here are similar at all observation sites. The Mount John values of r_0 are considerably smaller than previously reported values[13] for the same data, corresponding to a much closer match to the atmospheric conditions observed at the time the data were captured. The results are also more consistent in that successive profiles produce comparable C_n^2 strengths, independent of the binary star separation or defocus distance used.

5. Conclusions

In this paper we have described and illustrated a modified generalized SCIDAR inversion technique for estimating $C_n^2(h)$ profiles. The technique was verified by simulation and was then used to estimate $C_n^2(h)$ profiles for two astronomical observation sites. The corresponding r_0 values calculated from these profiles appear to better match the observed conditions than previously reported results from some of the same data. There is also an improved consistency in the r_0 values returned.

The modified normalization and inversion combines the generalized SCIDAR geometry with an accelerated quadratic programming method that uses an alternative weighting of the normalization. Representative solutions are achieved for small amounts of regularization. Finally, we confirmed the reliability of the method numerically by estimating the rms error between the true and the reconstructed $C_n^2(h)$ profiles.

We thank all the observatory staff who helped in the preparation of our observations at the 1-m McLellan telescope at Mount John and the 1.23-m telescope at Calar Alto. The Visiting Astronomer, German–Spanish Astronomical Centre, Calar Alto, is operated by the Max-Planck-Institute for Astronomy, Heidelberg, jointly with the Spanish National Commission for Astronomy. This study is supported by Particle Physics and Astronomy Research Council (PPARC) grants PPA/G/S/1997/00779 and PPA/G/S/1997/00289. It is also supported by The Paul Instrument Fund.

References

1. A. Tokovinin, M. le Louan, and E. Viard, "Optimized modal tomography in AO," Astron. Astrophys. **378,** 710–721 (2001).
2. T. Berkefeld, A. Glindemann, and S. Hippler, "Possibilities and performance of multi-conjugate adaptive optics," presented at AAS Meeting 194 (American Astronomical Society, Washington, D.C., 1999).
3. J. Vernin and F. Roddier, "Experimental determination of two-dimensional spatiotemporal power spectra of stellar light scintillation: evidence for a multilayer structure of the air turbulence in the upper troposphere," J. Opt. Soc. Am. **63,** 270–273 (1973).
4. A. Fuchs, M. Tallon, and J. Vernin, "Folding of the vertical atmospheric turbulence profile using an optical technique of movable observing plane," in *Atmospheric Propagation and Remote Sensing III*, W. A. Flood and W. B. Miller, eds., Proc. SPIE **2222,** 682–692 (1994).
5. R. Avila, J. Vernin, and E. Masciadri, "Whole atmospheric-turbulence profiling with generalized scidar," Appl. Opt. **36,** 7898–7905 (1997).
6. V. A. Kluckers, N. J. Wooder, T. W. Nicholls, M. A. Adcock, I. Munro, and J. C. Dainty, "Profiling of atmospheric turbulence strength and velocity using a generalised scidar technique," Astron. Astrophys. Suppl. Ser. **130,** 141–155 (1998).
7. R. Avila, J. Vernin, and L. J. Sanchez, "Atmospheric turbulence and wind profiles monitoring with generalized scidar," Astron. Astrophys. **369,** 364–372 (2001).
8. http://www.mpia-hd.mpg.de/AO/ATMOSPHERE/SCIDAR/SCIDARIntro.html
9. F. Roddier, "Effects of atmospheric turbulence in optics astronomy," in *Progress in Optics*, E. Wolf, ed. (Elsevier, Amsterdam, 1981), Vol. 19, pp. 281–376.
10. R. A. Johnston and R. G. Lane, "Estimating turbulence profiles in the atmosphere," in *Image Reconstruction from Incomplete Data*, M. A. Fiddy and R. P. Millane, eds., Proc. SPIE **4123,** 35–46 (2000).
11. G. A. Tyler and K. E. Steinhoff, "Scidar: measurement characteristics and noise amplification properties," tOSC Report TR-755R (Optical Sciences Co., Placentia, Calif., 1987).
12. R. A. Johnston, T. J. Connolly, and R. G. Lane, "An improved method for deconvolving a positive image," Opt. Commun. **181,** 267–278 (2000).
13. R. A. Johnston and R. G. Lane, "Results from Mount John SCIDAR experiments," in *Proceedings of Image and Vision Computing New Zealand*, IVCNZ'99, D. Pairman and H. North, eds. (University of Canterbury, Christchurch, New Zealand, 1999), pp. 271–276.